JACS
JOURNAL OF THE AMERICAN CHEMICAL SOCIETY
Communication
pubs.acs.org/JACS

Efficient Inorganic–Organic Hybrid Perovskite Solar Cells Based on Pyrene Arylamine Derivatives as Hole-Transporting Materials

Nam Joong Jeon,[†] Jaemin Lee,[†] Jun Hong Noh,[†] Mohammad Khaja Nazeeruddin,[‡] Michael Grätzel,[‡] and Sang Il Seok*[,†,∥]

[†]Division of Advanced Materials, Korea Research Institute of Chemical Technology, 141 Gajeong-Ro, Yuseong-Gu, Daejeon 305-600, Republic of Korea

[‡]Laboratory for Photonics and Interfaces, Institute of Chemical Sciences and Engineering, School of Basic Science, Swiss Federal Institute of Technology, CH-1015 Lausanne, Switzerland

[∥]Department of Energy Science, Sungkyunkwan University, Suwon 440-746, Korea

Supporting Information

ABSTRACT: A set of three *N*,*N*-di-*p*-methoxyphenylamine-substituted pyrene derivatives have successfully been synthesized and characterized by $^{1}H/^{13}C$ NMR spectroscopy, mass spectrometry, and elemental analysis. The optical and electronic structures of the pyrene derivatives were adjusted by controlling the ratio of *N*,*N*-di-*p*-methoxyphenylamine to pyrene, and investigated by UV/vis spectroscopy and cyclic voltammetry. The pyrene derivatives were employed as hole-transporting materials (HTMs) in fabricating mesoporous $TiO_2/CH_3NH_3PbI_3$/HTMs/Au solar cells. The pyrene-based derivative Py-C exhibited a short-circuit current density of 20.2 mA/cm^2, an open-circuit voltage (V_{oc}) of 0.886 V, and a fill factor of 69.4% under an illumination of 1 sun (100 mW/cm^2), resulting in an overall power conversion efficiency of 12.4%. The performance is comparable to that of the well-studied spiro-OMeTAD, even though the V_{oc} is slightly lower. Thus, this newly synthesized pyrene derivative holds promise as a HTM for highly efficient perovskite-based solar cells.

Fossil fuel consumption results in greenhouse gas production, which in turn causes global warming; therefore, the demand for carbon-free energy sources has increased. Solar energy is the largest source of carbon-free energy that can be converted into other forms of energy, such as heat and electricity. The use of solar cells is the most effective way to convert sunlight directly into electricity. Even though single-crystalline silicon-based solar cells are still used, great efforts to fabricate cost-effective and high-efficiency solar cells are being investigated. Novel approaches include solid-state dye-sensitized solar cells,[1] organic solar cells,[2] and inorganic–organic hybrid heterojunction solar cells using inorganic nanocrystalline semiconductors and quantum dots.[3]

Very recently, methylammonium lead halide ($CH_3NH_3PbX_3$, where X corresponds to halogens) perovskites were introduced as promising light harvesters in solar cells.[4] When $CH_3NH_3PbI_3$ (= $MAPbI_3$) was loaded on a mesoporous (mp)-TiO_2 electrode in conjunction with 2,2′,7,7′-tetrakis(*N*,*N*-di-*p*-methoxyphenylamine)-9,9′-spirobifluorene (spiro-OMeTAD) as the hole-transporting material (HTM), a 15.0% power conversion efficiency (η) was achieved under 1 sun (100 mW/cm^2) illumination.[4f] Snaith and co-workers[4g] showed a maximum performance of η = 15.4%, with an open-circuit voltage (V_{oc}) of 1.07 V and a short-circuit current density (J_{sc}) of 21.5 mA cm^{-2}, based on $CH_3NH_3PbI_{3-x}Cl_x$ deposited as thin layers with spiro-OMeTAD as the hole conductor. In mesoscopic solar cells using perovskites, several conducting polymers such as poly(3-hexylthiophene) (P3HT), poly[*N*-9-heptadecanyl-2,7-carbazole-*alt*-3,6-bis(thiophen-5-yl)-2,5-dioctyl-2,5-dihydropyrrolo[3,4]pyrrole-1,4-dione] (PCBTDPP), poly[2,1,3-benzothiadiazole-4,7-diyl[4,4-bis(2-ethylhexyl)-4*H*-cyclopenta[2,1-*b*:3,4-*b*′]dithiophene-2,6-diyl]] (PCPDTBT), poly[[9-(1-octylnonyl)-9*H*-carbazole-2,7-diyl]-2,5-thiophenediyl-2,1,3-benzothiadiazole-4,7-diyl-2,5-thiophenediyl] (PCDTBT), and poly(triarylamine) (PTAA) have been used as HTMs.[4d,e,h] However, the high cost of HTMs and/or low performance hinders the advancement of cost-effective and practical perovskite solar cells.

As mentioned above, it has been demonstrated that spiro-OMeTAD is an effective small-molecule HTM for perovskite solar cells. However, the spirobifluorene core in the spiro-OMeTAD molecule is relatively expensive due to extensive synthetic processes for its preparation. So it would be of importance to develop a cheaper alternative to spiro-OMeTAD for successful commercialization of hybrid perovskite solar cells. The pyrene core deserves attention in that regard, because it can be isolated from coal tar or produced in a wide range of combustion conditions. Pyrene has fast charge-transport ability due to its strong electron delocalization character that is a result of the four fused benzene rings of an alternate polycyclic aromatic hydrocarbon. Because pyrene can be substituted with a range of functional groups, pyrene-core derivatives are useful as HTMs.[5] However, the synthesis of *N*,*N*-di-*p*-methoxyphenylamine-substituted pyrene derivatives and their application as HTMs in perovskite-based solar cells have not yet been reported.

In this work, we report the synthesis and characterization of three pyrene-core arylamine derivatives, and their application in perovskite-based solar cells. The spirobifluorene core of spiro-OMeTAD was replaced with a pyrene core. The role of the

Received: October 18, 2013
Published: December 6, 2013

dx.doi.org/10.1021/ja410659k | J. Am. Chem. Soc. 2013, 135, 19087–19090

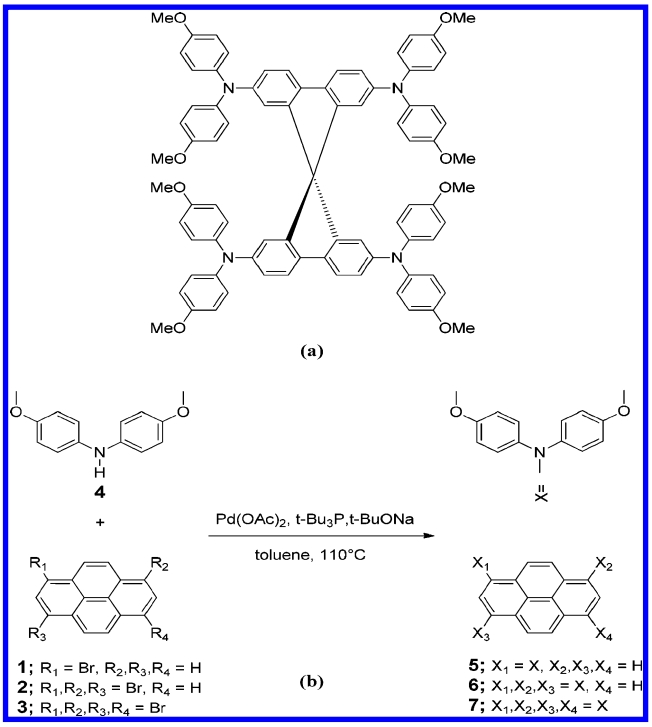

Figure 1. (a) Structures of spiro-OMeTAD. (b) Synthetic routes for pyrene arylamine derivatives.

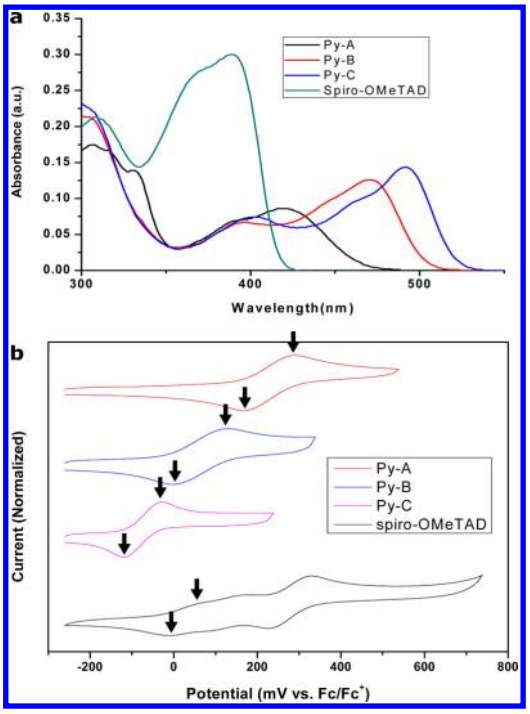

Figure 2. (a) UV/vis absorption spectra of Py-A, Py-B, Py-C, and spiro-OMeTAD in chlorobenzene. (b) Cyclic voltammograms of Py-A, Py-B, Py-C, and spiro-OMeTAD. Square wave voltammetry (SWV) was carried out at a step potential of 4 mV, square wave amplitude of 25 mV, and square wave frequency of 15 Hz, at a scan rate of 40 mV/s with ferrocene as the internal standard. Scan rate was 100 mV/s.

methoxy group in the *N*,*N*-di-*p*-methoxyphenylamine substituent is to adjust the electronic properties of the hole conductor. The cells, fabricated using one of the pyrene derivatives as a HTM, showed a PCE of 12.4% under AM 1.5 G illumination at 100 mW/cm^2; this is one of the highest PCE values reported to date for mp-TiO_2/$CH_3NH_3PbI_3$ perovskite/small-molecule HTM with the exception of spiro-OMeTAD.

The procedures for the synthesis of the pyrene arylamine derivatives are shown in Figure 1, and experimental details are given in the Supporting Information (SI).

A triarylamine unit containing a *para*-substituted methoxy functional group was synthesized by the Buchwald–Hartwig amination reaction,[6] carried out between various bromopyrene derivatives and dimethoxydiphenylamines under the modified reaction conditions. Mono-, tri-, and tetra-substituted pyrenes were then successfully purified by column chromatography and recrystallization. The new pyrene arylamine derivatives **5**, **6**, and **7** (denoted as Py-A, Py-B, and Py-C, respectively) were fully characterized by ^{1}H/^{13}C NMR spectroscopy, mass spectrometry, and elemental analysis (see the SI). It was observed that the ^{1}H NMR spectrum of the tetra-substituted Py-C is very simple due to its symmetric structure. The Py-C spectrum show two singlets at δ = 7.88 and 7.43 ppm, corresponding to the pyrene ring protons at positions 4, 5, 9, and 10, and positions 2 and 7 in a 2:1 ratio, respectively. A pair of doublets in 1:1 ratio at δ = 6.85 and 6.67 ppm for the aromatic protons and a singlet at δ = 3.71 ppm for the eight methoxy group protons are also observed. Py-A and Py-B structures were also confirmed by ^{1}H NMR via proton integration and chemical shift identification of the substituted pyrenes. In addition, the structures of Py-A, Py-B, and Py-C were further established by mass spectrometry and their respective molecular ion ([M$^+$]) peaks: 429 for Py-A, 883 for Py-B, and 1110 for Py-C. Finally, we confirmed the structures by elemental analysis, where the experimental ratios of nitrogen, carbon, and proton agreed well with the expected ratios. All the analytical data were consistent with the proposed structures. The three compounds have good solubility in all common organic solvents. The solubility of the pyrene arylamine derivatives decreased with an increase in the number of di-*p*-methoxyphenylamino substituents.

The UV/vis absorption spectra of Py-A, Py-B, and Py-C in chlorobenzene are shown in Figure 2a. All derivatives show absorption bands in the visible region, in contrast to spiro-OMeTAD that shows an absorption band in the UV region. The absorption maxima of Py-A, Py-B, and Py-C are centered at 420, 470, and 492 nm, respectively. This is due to the electron-donating effect of the diphenylamine group, which is directly bonded to the pyrene core and increases the electron density in the pyrene core. Thus, the increased electron density modifies the position of the highest occupied molecular orbital (HOMO) and the lowest unoccupied molecular orbital (LUMO), and the gap between them. The energy level of the compounds was characterized by cyclic voltammetry (CV, see Figure 2b). All CV measurements were carried out in freshly distilled 1,2-dichlorobenzene using 1 mM tetrabutylammonium hexafluorophosphate ($TBAPF_6$) as electrolyte in a three-electrode system, and each solution was purged with N_2 prior to measurement. The working electrode, the reference electrode, and the counterelectrodes were a Pt disk, Ag/AgCl, and Pt rods, respectively. All measurements were carried out at room temperature using a μAUTOLAB Type III potentiostat, employing the electrochemical software GPES. The optical properties and electrochemical data of Py-A, Py-B, and Py-C with regard to spiro-OMeTAD were obtained by UV/vis spectroscopy and CV measurement; the results are summarized in Table 1.

We compared the photovoltaic performance of the perovskite-based solar cells fabricated using the three types of pyrene

dx.doi.org/10.1021/ja410659k | *J. Am. Chem. Soc.* 2013, 135, 19087–19090

Table 1. Summary of the Optical and Electrochemical Properties[a]

	λ_{max} (nm)[a]	E_{gap} (eV)[b]	E_{pc} (mV)[c]	E_{pa} (mV)[c]	$E_{ox,1/2}$ (mV)[c]	E_{HOMO} (eV)[c]	E_{LUMO} (eV)[d]
Py-A	420	2.63	292	166	229	-5.41	-2.78
Py-B	470	2.43	133	-1	66	-5.25	-2.82
Py-C	492	2.36	-28	-119	-74	-5.11	-2.74
Spiro-OMeTAD	388	2.95	83	-9	37	-5.22	-2.27

[a]E_{HOMO} and E_{LUMO} values obtained by comparison with spiro-OMeTAD. [b]From absorption at λ_{max}. [c]From intersection of absorption spectra. [d]From CV measurements and referenced to ferrocene. [e]$E_{LUMO} = E_{HOMO} + E_{gap}$.

derivatives (Py-A, Py-B, Py-C), and the spiro-OMeTAD as HTMs, with tris[2-(1*H*-pyrazol-1-yl)-4-*tert*-butylpyridine)-cobalt(III) tris(bis(trifluoromethylsulfonyl)imide)] (FK209), lithium bis(trifluoromethanesulfonyl)imide (Li-TFSI), and 4-*tert*-butylpyridine (tBP) as additives, dissolved in toluene. Here, FK209 (co-complex) was used because it increased the performance of the perovskite-based solar cell.[7] The concentration of HTMs was also adjusted in the range of 12.5−25.0 mM to control the overlayer thickness on the perovskite. Finally, gold as a top electrode for each cell was chosen and deposited by thermal evaporation because its work function is close to the HOMO of the pyrene derivatives. As shown in Figure 3a, the

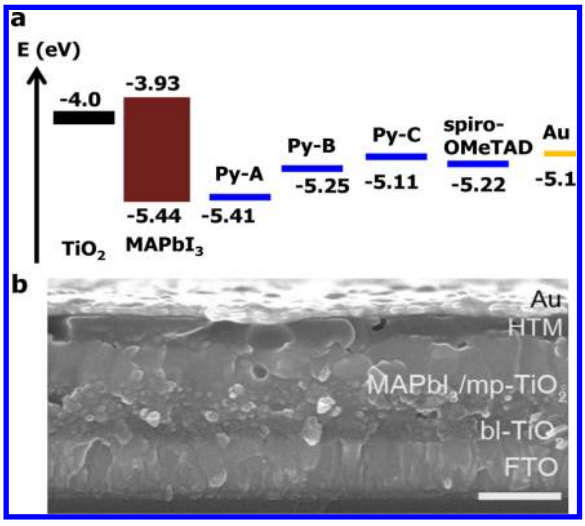

Figure 3. (a) Energy level diagram of the corresponding materials used in our devices. (b) Cross-sectional structure of the representative device. Scale bar = 500 nm.

HOMO levels of Py-A, Py-B, and Py-C are ∼−5.41, −5.25, and −5.11 eV, respectively. The band alignment in TiO_2, $MAPbI_3$, and pyrene derivatives is such that exciton dissociation and charge transfer at the interface are energetically favorable. Hence, a driving force may possibly be generated for hole transfer from the $MAPbI_3$ into the pyrene derivatives. Figure 3b compares cross-sectional images, as observed by scanning electron microscopy, of the representative solar cell device. The image shows a device thickness of ∼670 nm, consisting of a $MAPbI_3$-deposited mesoporous layer (∼600 nm) that is uniformly capped by a HTM overlayer of pyrene arylamine derivative (∼70 nm). Here, the thickness of HTMs can be controlled by adjusting the

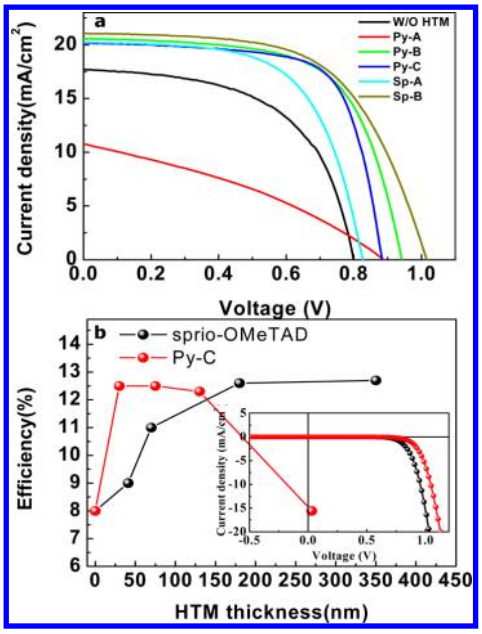

Figure 4. (a) Current density−voltage (J−V) curves for TiO_2/$MAPbI_3$/HTMs/Au fabricated with Py-A, Py-B, Py-C, Sp-A, and Sp-B as HTMs, and without HTM. (b) The efficiency dependence on the overlayer thickness with Py-C and spiro-OMeTAD; inset is dark J−V curves for Py-C and Sp-B devices.

solution concentration for HTMs. The gold contact on top of this organic conductor is also observed.

Figure 4a shows current density−voltage (J−V) curves for TiO_2/$MAPbI_3$/HTMs/Au solar cells fabricated using Py-A, Py-B, and Py-C as HTMs. The photovoltaic parameters for these devices are summarized in Table 2. For comparison, cells without

Table 2. Summary of Short-Circuit Current Densities, Open-Circuit Voltages, Fill Factors, and Overall Conversion Efficiencies Obtained from the Device Shown in Figure 4a[a]

HTM	J_{sc} (mA cm^{-2})	V_{oc} (V)	FF (%)	η (%)	R_s (Ω)
without	17.7	0.80	56.5	8.0	65.6
Py-A	10.8	0.89	34.6	3.3	402.2
Py-B	20.4	0.95	63.7	12.3	64.3
Py-C	20.2	0.89	69.4	12.4	51.6
Sp-A	20.2	0.83	61.8	10.3	64.6
Sp-B	21.0	1.01	59.5	12.7	85.9

[a]Masks (0.092 cm^2) made of thin metal were attached to each cell before measurement.

a HTM and with spiro-OMeTAD were also fabricated. In the case of spiro-OMeTAD, ∼70 and ∼180 nm overlayer thicknesses were compared, denoted as Sp-A, and Sp-B, respectively). The device comprising mp-TiO_2/$MAPbI_3$/Au without a HTM gives V_{oc} = 800 mV, J_{sc} = 17.7 mA cm^{-2}, a fill factor (FF) of 56.5%, and an overall conversion efficiency η = 8.0%. These values are similar to those recently reported by Etgar et al.[8] In contrast, mp-TiO_2/$MAPbI_3$/HTMs/Au devices exhibit dramatically enhanced performance, depending on the HTMs, with the exception of the cell fabricated with Py-A as HTM. The low performance shown by Py-A is mainly related to the insufficient driving force for hole injection owing to a low offset in the energy level between $MAPbI_3$ and Py-A (see Table 2). In addition, the cell fabricated with Sp-A exhibits a low V_{oc} = 0.83 V relative to those of Py-B and Py-C showing a same thickness as that of Sp-B.

dx.doi.org/10.1021/ja410659k | J. Am. Chem. Soc. 2013, 135, 19087−19090

Figure 4b shows the PCEs for the cells fabricated as a function of overlayer thickness for Py-C and spiro-OMeTAD. The cells fabricated with Py-C show a maximum PCE at a relatively thinner overlayer thickness than 100 nm. On the other hand, spiro-OMeTAD has shown a maximum efficiency in relatively thicker cells than 180 nm in overlayer thickness. The cells fabricated using the thicker spiro-OMeTAD are similar with the average performance reported by M. Gratzel et al.[4f] The values of J_{sc} for the cells fabricated with Py-B, Py-C, Sp-A, and Sp-B are 20.4, 20.2, 20.2, and 21.0 mA cm^{-2}, respectively. This indicates that there is a small difference in the charge collection of the HTMs (Py-B, Py-C, Sp-A, and Sp-B). We also see the enhancement of the V_{oc} values in the sequence of Sp-A, Py-C, Py-B, and Sp-B. The difference in V_{oc} for the cells fabricated with Py-B and Py-C as HTMs agrees with the relative difference in the HOMO levels of the two HTMs because the photovoltage is determined by the difference in the quasi-Fermi level of the electrons in the TiO_2 and the quasi-Fermi level of the holes in the hole conductor. The higher V_{oc} value observed in Sp-B might be attributed to the effective movement of electrons from the HOMO of spiro-OMeTAD to the Co-complex, which is used as dopant, inducing a lower shift in the Fermi level to the HOMO of spiro-OMeTAD.[7] In addition, the V_{oc} may be attributed the charge recombination kinetics. Diode-like current−voltage (I−V) characteristics in the dark can give an evident insight into the charge recombination in the real device. As shown in the inset of Figure 4b, the cell with Py-C has a relatively lower dark current and an upper shift in the onset, compared to Py-C. This implies that Py-C has an electron-blocking ability superior to that of spiro-OMeTAD. Thus, it would be effective to reduce the use of expensive HTMs. However, the dependence of the V_{oc} on the HTMs may be attributed to several factors and will require additional study. Figure 4a and Table 2 show that comparable performance of Py-C and Sp-B as HTMs is due to the enhanced FF despite the difference in their J_{sc}'s and V_{oc}'s. The FF is related to series resistance (R_s) and shunt resistance (R_{sh}). In order to obtain a high FF, the solar cells should have a low R_s and a high R_{sh}. In other words, the HTM layer should effectively block the electron and transport the hole from $MAPbI_3$ to the Au electrode. The main difference between the cells studied here is the HTM, as the configurations of the cells are similar with regard to the thickness of the overlayers below the Au electrode (see Figure 3b). This means that the FF value can partly be explained by the increased hole-transporting and electron-blocking ability of the HTMs, which would decrease the possibility for the photogenerated charges to recombine before they reach the contacts. From the J−V curves under a condition of 1 sun, the Py-B- and Py-C-based cells showed R_s = 64.26 and 51.57 Ω, respectively, whereas the spiro-OMeTAD had R_s = 85.87 Ω. Therefore, the pyrene-core HTM, especially Py-C, exhibited a better FF than the spiro-OMeTAD.

In summary, we synthesized pyrene-core arylamine derivatives that were applied in solar cells as HTMs. On the basis of the CV measurements and UV/vis spectra, the HOMO/LUMO of the pyrene-core arylamine derivatives were characterized for use as HTMs. The derivatives were used to fabricate feasible perovskite solar cells. Energy conversion efficiencies of 12.4% and 12.7% were measured for the devices with Py-C and spiro-OMeTAD as HTM. We believe that pyrene-core arylamine derivatives can be used as HTMs for the fabrication of efficient and cost-effective photovoltaic devices.

■ ASSOCIATED CONTENT

Supporting Information

Experimental details and additional figures. This material is available free of charge via the Internet at http://pubs.acs.org.

■ AUTHOR INFORMATION

Corresponding Author

seoksi@krict.re.kr (seoksi@skku.edu)

Notes

The authors declare no competing financial interest.

■ ACKNOWLEDGMENTS

This study was supported by the Global Research Laboratory (GRL) Program and the Global Frontier R&D Program on Center for Multiscale Energy System funded by the National Research Foundation under the Ministry of Science, ICT & Future, Korea, and by a grant from the KRICT 2020 Program for Future Technology of the Korea Research Institute of Chemical Technology (KRICT), Republic of Korea.

■ REFERENCES

(1) (a) Burschka, J.; Dualeh, A.; Kessler, F.; Baranoff, E.; Cevey-Ha, N.-L.; Yi, C.; Nazeeruddin, M. K.; Gratzel, M. *J. Am. Chem. Soc.* **2011**, *133*, 18042. (b) Chung, I.; Lee, B.; He, J.; Chang, R. P. H.; Kanatzidis, M. G. *Nature* **2012**, *485*, 486. (c) Zhang, W.; Zhu, R.; Li, F.; Wang, Q.; Liu, B. *J. Phys. Chem. C* **2011**, *115*, 7038.

(2) (a) Sun, Y.; Welch, G. C.; Leong, W. L.; Takacs, C. J.; Bazan, G. C.; Heeger, A. J. *Nat. Mater.* **2012**, *11*, 44. (b) Li, G.; Zhu, R.; Yang, Y. *Nat. Photon.* **2012**, *6*, 153. (c) Zhou, J.; Zuo, Y.; Wan, X.; Long, G.; Zhang, Q.; Ni, W.; Liu, Y.; Li, Z.; He, G.; Li, C.; Kan, B.; Li, M.; Chen, Y. *J. Am. Chem. Soc.* **2013**, *135*, 8484.

(3) (a) Sangtra, P. K.; Kamat, P. V. *J. Am. Chem. Soc.* **2012**, *134*, 2508. (b) Lee, Y. H.; Im, S. H.; Rhee, J. H.; Lee, J.-H.; Seok, S. I. *ACS Appl. Mater. Interfaces* **2010**, *2*, 1648. (c) Chang, J. A.; Rhee, J. H.; Im, S. H.; Lee, Y. H.; Kim, H.-J.; Seok, S. I.; Nazeeruddin, M. K.; Grätzel, M. *Nano Lett.* **2010**, *10*, 2609. (d) Im, S. H.; Lim, C.-S.; Chang, J. A.; Lee, Y. H.; Maiti, N.; Kim, H.-j.; Nazeeruddin, Md. K.; Grätzel, M.; Seok, S. I. *Nano Lett.* **2011**, *11*, 4789. (e) Chang, J. A.; Im, S. H.; Lee, Y. H.; Kim, H.-j.; Lim, C.-S.; Heo, J. H.; Seok, S. I. *Nano Lett.* **2012**, *12*, 1863. (f) Im, S. H.; Kim, H.-j.; Kim, S. W.; Kim, S.-W.; Seok, S. I. *Energy Environ. Sci.* **2011**, *4*, 4181.

(4) (a) Kojima, A.; Teshima, K.; Shirai, Y.; Miyasaka, T. *J. Am. Chem. Soc.* **2009**, *131*, 6050. (b) Lee, M. M.; Teuscher, J.; Miyasaka, T.; Murakami, T. N.; Snaith, H. J. *Science* **2012**, *338*, 643. (c) Kim, H.-S.; Lee, C.-R.; Im, J.-H.; Lee, K.-B.; Moehl, T.; Marchioro, A.; Moon, S.-J.; Humphry-Baker, R.; Yum, J.-H.; Moser, J. E.; Grätzel, M.; Park, N.-G. *Sci. Rep.* **2012**, *2*, 591:1-7. (d) Heo, J. H.; Im, S. H.; Noh, J. H.; Mandal, T. N.; Lim, C.-S.; Chang, J. A.; Lee, Y. H.; Kim, H.; Sarkar, A.; Nazeeruddin, M. K.; Grätzel, M.; Seok, S. I. *Nat. Photon.* **2013**, *7*, 486. (e) Noh, J. H.; Im, S. H.; Heo, J. H.; Mandal, T. N.; Seok, S. I. *Nano Lett.* **2013**, *13*, 1764. (f) Burschka, J.; Pellet, N.; Moon, S.-J.; Humphry-Baker, R.; Gao, P.; Nazeeruddin, M. K.; Grätzel, M. *Nature* **2013**, *499*, 316. (g) Liu, M.; Johnston, M. B.; Snaith, H. J. *Nature* **2013**, *501*, 395. (h) Cai, B.; Xing, Y.; Yang, Z.; Zhang, W.-H.; Qiu, J. *Energy Environ. Sci* **2013**, *6*, 1480.

(5) (a) Haedler, A. T.; Misslitz, H.; Buehlmeyer, C.; Albuquerque, R. Q.; Köhler, A.; Schmidt, H.-W. *ChemPhysChem* **2013**, *14*, 1818. (b) Anant, P.; Lucas, N. T.; Ball, J. M.; Anthopoulos, T. D.; Jacob, J. *Synth. Met.* **2010**, *160*, 1987.

(6) Thomas, K. R.; Lin, J. T.; Tao, Y.-T.; Ko, C.-W. *J. Am. Chem. Soc.* **2001**, *123*, 9404.

(7) Noh, J. H.; Jeon, N. J.; Choi, Y. C.; Nazeeruddin, M. K.; Grätzel, M.; Seok, S. I. *J. Mater. Chem. A* **2013**, *1*, 11842.

(8) Laban, W. A.; Etgar, L. *Energy Environ Sci.* **2013**, *6*, 3249.